

Comparison of the X-ray structure of native rubredoxin from *Pyrococcus furiosus* with the NMR structure of the zinc-substituted protein



PAUL R. BLAKE,¹ MICHAEL W. DAY,² BARBARA T. HSU,² LEEMOR JOSHUA-TOR,²
JAE-BUM PARK,³ DENNIS R. HARE,⁴ MICHAEL W.W. ADAMS,³
DOUGLAS C. REES,² AND MICHAEL F. SUMMERS¹

¹ Department of Chemistry and Biochemistry, University of Maryland Baltimore County, Baltimore, Maryland 21228

² Division of Chemistry and Chemical Engineering, California Institute of Technology, Pasadena, California 91125

³ Department of Biochemistry and Center for Metalloenzyme Studies, University of Georgia, Athens, Georgia 30602

⁴ Hare Research, Inc., 18943 120th Avenue N.E., Bothell, Washington 98011

(RECEIVED April 29, 1992; REVISED MANUSCRIPT RECEIVED June 19, 1992)

Abstract

The three-dimensional X-ray structures of the oxidized and reduced forms of rubredoxin from *Pyrococcus furiosus*, determined at -161°C , and the NMR structure of the zinc-substituted protein, determined in solution at 45°C , are compared. The NMR and X-ray structures, which were determined independently, are very similar and lead to similar conclusions regarding the interactions that confer hyperthermostability.

Keywords: distance geometry; hyperthermophile; iron-sulfur protein; NMR structure; protein structure; rubredoxin; X-ray structure; zinc substitution

The two companion papers (this issue: Blake et al., 1992; Day et al., 1992) describe X-ray and NMR structure determinations of rubredoxin (Rd) from the hyperthermophilic archaeobacterium *Pyrococcus furiosus*. X-ray structure analyses were performed on the oxidized and reduced forms of the protein (Rd-ox and Rd-red) at -161°C , and NMR studies were performed on the zinc-substituted form of the protein (Zn(Rd)) in solution at 45°C . In this paper, we briefly compare the results of the X-ray and NMR structural studies.

Discussion

As indicated in Blake et al. (1992) and Day et al. (1992), the NMR and X-ray structures of *P. furiosus* Rd were found to be conformationally similar to the X-ray structure of Rd from the mesophile *Clostridium pasteurianum*. Thus, as expected, the X-ray structures of *P. furiosus* Rd-ox and Rd-red and the NMR structure of the Zn(Rd) are also similar to each other. Superposition of the back-

bone C, C α , and N atoms of residues A1–L51 of the 40 independently generated NMR structures (Zn(Rd)) with the X-ray structures of native Rd-ox and Rd-red afforded pairwise root mean square (rms) deviation values of $0.69 \pm 0.07 \text{ \AA}$ and $0.69 \pm 0.06 \text{ \AA}$, respectively (Fig. 1; Table 1; Kinemage 1). By comparison, the mean rms deviation among the same atoms of the NMR structures alone is $0.42 \pm 0.07 \text{ \AA}$ (with maximum and minimum rms deviations = 0.64 \AA and 0.23 \AA , respectively), and the deviation between the two X-ray structures is 0.14 \AA . The rms deviations between these atoms of Rd-ox and Rd-red and the mean NMR coordinates are 0.62 \AA and 0.63 \AA , respectively. Thus, the rms deviation of the backbone atoms for residues A1–L51 of the X-ray and NMR structures is just slightly greater (0.20 \AA) than the rms deviations among the NMR structures alone.

The only notable differences involving the backbone atoms of the NMR and X-ray structures occur at the C-terminal residues. Whereas the NMR data indicate that residues Glu 52 and Asp 53 exist in rapid dynamic equilibrium in solution (as reflected by the high deviations in the C α positions; Fig. 2), in crystals the conformations of these residues are restricted due to their involvement in lattice contacts. Even so, there is evidence for confor-

Reprint requests to: Michael F. Summers, Department of Chemistry and Biochemistry, University of Maryland Baltimore County, Baltimore, Maryland 21228.

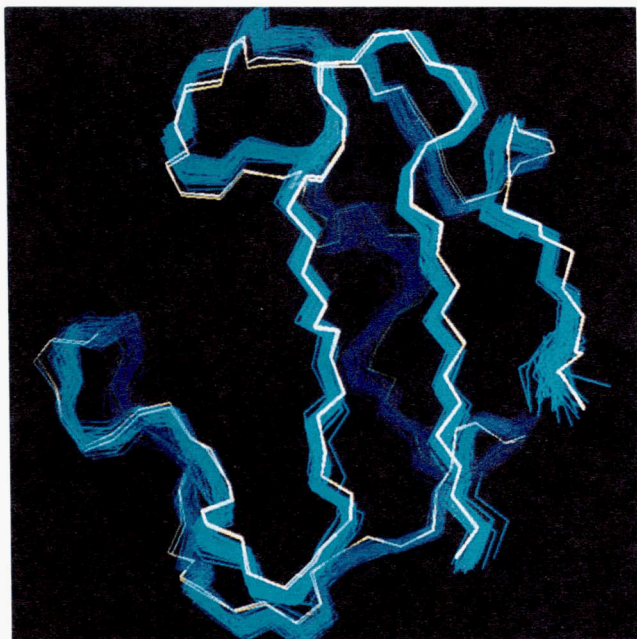


Fig. 1. Superposition of the C, C α , and N backbone atoms of 40 distance geometry/simulated annealing determined (DG/SA) NMR structures of *Pyrococcus furiosus* zinc-substituted rubredoxin (blue) with the X-ray structures of the native oxidized (white) and reduced (yellow) proteins.

mational variability at the C-terminus, because the backbone conformations of these residues in the oxidized and reduced proteins differ slightly, the B -values for the C α carbons of these residues are two- to threefold larger than the mean B -values (Fig. 2), and multiple side-chain conformations were observed for E52 and D53 in the X-ray

structure of the oxidized protein. Thus the NMR findings that these residues are conformationally labile in solution are not unexpected and are fully compatible with the X-ray data. Interestingly, variations in the B -values of the C α carbons observed for the reduced protein generally parallel the C α deviations observed in the NMR structures (Fig. 2).

The hydrophobic residues in the core of the NMR and X-ray models are also packed in a similar fashion (Fig. 3; Kinemage 2). Superposition of all heavy atoms of residues A1–L51, which included external residues that are conformationally undefined in the NMR structures, afforded pairwise rms deviation values of 1.13 ± 0.07 Å and 1.14 ± 0.06 Å for Rd-ox and Rd-red, respectively. Both models present hydrogen bonds and potential electrostatic interactions unique to this class of protein (Fig. 4; Kinemage 3).

The surface residues can be grouped into two categories: those that contain hydrophobic and those that contain hydrophilic side chains. Good agreement was generally observed for the side chains of the exposed hydrophobic residues (V4, I7, I11, A16, I23, V37, I40). The only notable exceptions occurred for the δ -methyl groups of the Ile residues. The NMR structures generally exhibited multiple orientations for the δ -methyl groups. Although quantitative comparisons have yet to be performed, analysis of the back-calculated nuclear Overhauser effect spectra (NOESY) suggests that, for I11 (at least), the X-ray models are more consistent with the experimental NOESY data than the NMR model. Studies with ^{13}C -labeled protein could allow identification of additional side chain–side chain NOEs that would define more precisely the orientation of these methyl groups.

Table 1. Statistics for the NMR and X-ray structures of *Pyrococcus furiosus* rubredoxin^a

Superpositioned residues	Rd-ox	Rd-red
Backbone atoms ^b		
5–10, 38–43 (metal site residues)	0.32 ± 0.03	0.33 ± 0.03
15–26	0.48 ± 0.11	0.46 ± 0.10
1–14, 27–51	0.64 ± 0.07	0.66 ± 0.07
1–51	0.69 ± 0.07	0.69 ± 0.06
Mean backbone coordinates ^c		
5–10, 38–43 (metal site residues)	0.29	0.31
15–26	0.42	0.40
1–14, 27–51	0.59	0.61
1–51	0.62	0.63
All heavy atoms ^d		
1–51	1.13 ± 0.07	1.14 ± 0.06

^a Mean pairwise rms deviation values (\pm SD) obtained upon superpositioning the 40 distance geometry/simulated annealing determined (DG/SA) NMR structures with the X-ray structures of rubredoxin (Rd) in its oxidized (Rd-ox) and reduced (Rd-red) states.

^b C, C α , and N atoms of 40 DG/SA structures.

^c Superposition of mean C, C α , and N coordinates of the 40 DG/SA structures.

^d Includes superposition of side-chain atoms that are structurally undefined in the 40 DG/SA NMR models.

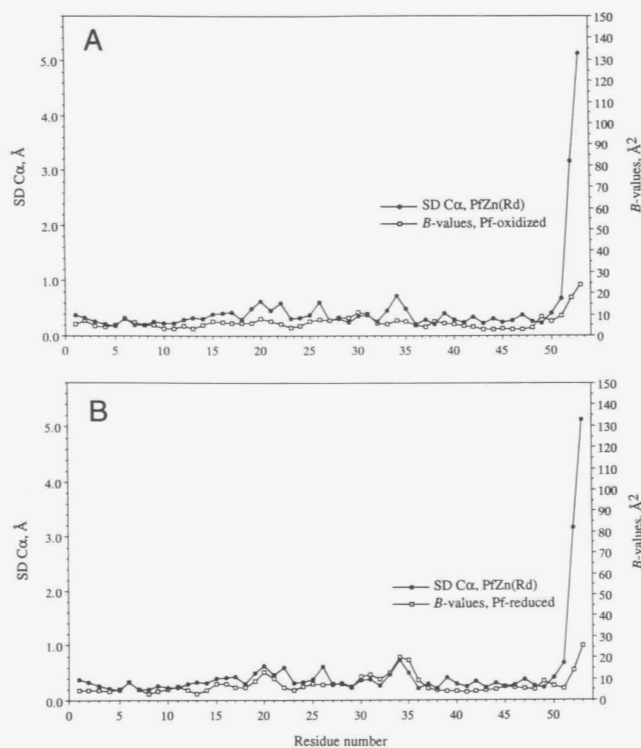


Fig. 2. Comparison between the crystallographic B -values of the $C\alpha$ carbons of oxidized (**A**) and reduced (**B**) *P. furiosus* rubredoxin and the standard deviation from the mean $C\alpha$ coordinates of the 40 DG/SA structures of zinc-substituted rubredoxin (Zn(Rd)). Large standard deviations associated with residues E52 and D53 reflect conformational disorder in solution.

In general, the longer side chains of the surface hydrophilic residues (K2, K6, K28, E30, E31, K45, E47, E49, K50) exhibited disorder in the NMR structures, and this is due to the lack of NOE restraints for protons beyond the $C\beta$ carbon. On the basis of the relative orientations of the charged surface residues observed in the NMR structures, potential electrostatic interactions were proposed to involve (1) K6 and E49 and/or E47, (2) K45 and E30 and/or D34, and (3) K28 and E31. Hydrogen bonding involving the side chains of K6:E49 and K45:F29(O) were observed in the X-ray structures. In general, orientations for the shorter side chains of surface hydrophilic residues D13, D15, D18, S24, T27, D34, D35, and S46 of the NMR structures agreed with the X-ray structures, the exceptions being the undefined $O\gamma$ atoms of the Ser residues. In addition, the $C\gamma$ carbons of the Asp residues were generally undefined in the NMR structures, except for the case of D13 where side-chain H-bonding was invoked. The orientations of the T27 side chains observed by NMR and X-ray crystallography were also in good agreement, due to NMR restraints involving the side-chain OH proton. In general, the hydrogen bonds identified in the NMR structures were also observed in the X-ray structures. A hydrogen bond between K45NH and W36O was proposed

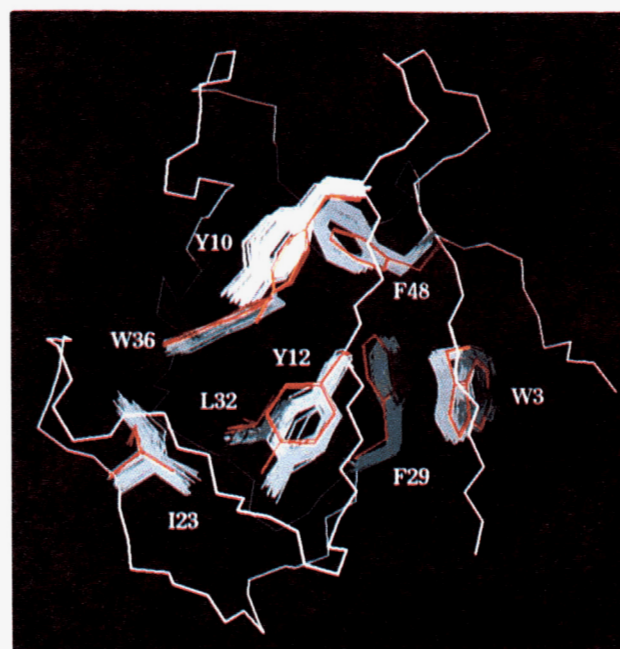


Fig. 3. Relative orientations of the hydrophobic residues of the 40 DG/SA NMR structures of *P. furiosus* Zn(Rd) (gray) and the X-ray structures of the native oxidized (red) and reduced (orange) proteins. Residues depicted include the six aromatic and two hydrophobic side chains of residues of W3, Y10, Y12, I23, L32, W36, and F48. This figure was generated by superpositioning the backbone C, $C\alpha$, and N atoms of residues A1–L51.

in the NMR structure (on the basis of slow NH exchange and several long-range NOEs) but not in the X-ray structures. Additional hydrogen bonds identified only in the X-ray structure include: E52N–K50O (E52 appeared to be

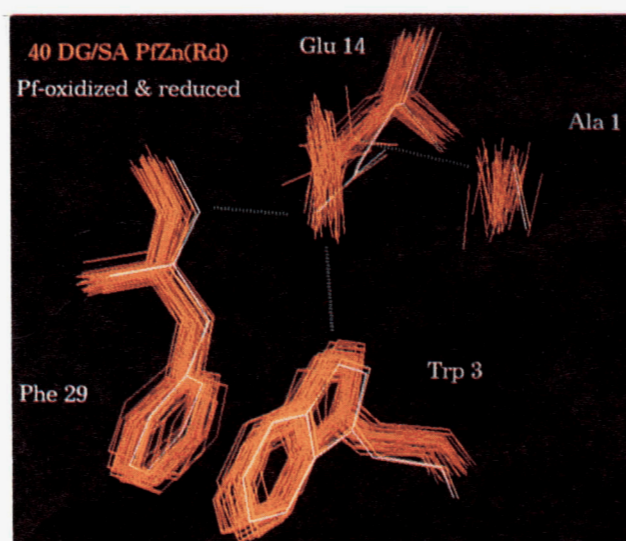


Fig. 4. Relative orientations of the groups proposed to form hydrogen bonds and salt bridges (green dashed lines) unique to *P. furiosus* rubredoxin on the basis of NMR and X-ray diffraction data. The display was achieved by superposition of the backbone C, $C\alpha$, and N atoms of residues A1–L51.

conformationally labile at 45 °C on the basis of the NMR data) and S46O γ -E47O ϵ 2.

The complementarity of the two approaches is illustrated most clearly by the combined effort to structurally characterize the Asn 21 side-chain hydrogen bond (Kinimage 4). NMR data clearly indicated that the side-chain NH ϵ proton of Asn 21 was involved in a hydrogen bond, and NOE information provided solid information on the relative orientation of the Asn 21 side-chain atoms. However, due to NH ϵ proton chemical exchange, the precise position of this side chain could not be established unambiguously. In addition, the orientation of the Asp 20 side-chain group could not be defined on the basis of NOE data due to chemical shift degeneracy of its H β , β' methylene protons. Thus, the side-chain carboxyl groups of both Asp 18 and Asp 20 were found to serve as potential H-bond acceptors for the Asn 21-NH ϵ proton. By comparison, the electron-density data clearly indicated that the Asp 18 side chain participates in hydrogen bonding

to the Asn 21 side chain. However, the nature of the hydrogen bond (i.e., Asp-COOH-to-Asn-CO δ versus Asp-COO $^-$ -to-Asn-NH ϵ) cannot be established on the basis of the diffraction data alone. Although the latter argument is more plausible chemically, the two possibilities cannot be experimentally distinguished in an X-ray diffraction study, since the electron densities of the Asn N δ and O δ atoms are virtually identical. The collective data define the hydrogen bond as Asn 21-NH ϵ to Asp 18-COO $^-$.

References

- Blake, P.R., Park, J.-B., Zhou, Z.H., Hare, D.R., Adams, M.W.W., & Summers, M.F. (1992). Solution-state structure by NMR of zinc-substituted rubredoxin from the marine hyperthermophilic archaeobacterium *Pyrococcus furiosus*. *Protein Sci.* 1, 1508-1521.
- Day, M.W., Hsu, B.T., Joshua-Tor, L., Park, J.-B., Zhou, Z.H., Adams, M.W.W., & Rees, D.C. (1992). X-ray crystal structures of the oxidized and reduced forms of the rubredoxin from the marine hyperthermophilic archaeobacterium *Pyrococcus furiosus*. *Protein Sci.* 1, 1494-1507.